

## Noise Characterization in InAlAs/InGaAs/InP pHEMTs for Low Noise Applications

Z. A. Djennati, K. Ghaffour

<sup>1</sup>Electronic and Electrical Engineering Department, University of Abu Bekr Belkaid Tlemcen, Algeria  
Research Unit of Materials and Renewable Energies

---

### Article Info

#### Article history:

Received Jul 10, 2016

Revised Sep 20, 2016

Accepted Oct 13, 2016

---

#### Keyword:

InAlAs/InGaAs/InP

LNA

Noise simulation

pHEMT

PRC model

---

### ABSTRACT

In this paper, a noise revision of an InAlAs/InGaAs/InP pseudomorphic high electron mobility transistor (pHEMT) is presented. The noise performances of the device were predicted over a range of frequencies from 1GHz to 100GHz. The minimum noise figure (NF<sub>min</sub>), the noise resistance (R<sub>n</sub>) and optimum source impedance (Z<sub>opt</sub>) were extracted using two approaches. A physical model that includes diffusion noise and G-R noise models and an analytical model based on an improved PRC noise model that considers the feedback capacitance C<sub>gd</sub>. The two approaches presented matched results allowing a good prediction of the noise behaviour. The pHEMT was used to design a single stage S-band low noise amplifier (LNA). The LNA demonstrated a gain of 12.6dB with a return loss coefficient of 2.6dB at the input and greater than -7dB in the output and an overall noise figure less than 1dB.

*Copyright © 2017 Institute of Advanced Engineering and Science.  
All rights reserved.*

---

### Corresponding Author:

Z. A. Djennati,

Electronic and Electrical Engineering Department,

University of Abu Bekr Belkaid Tlemcen,

22 Abi Ayed Abdelkrim Road, Tlemcen, 13000, Algeria

Email: zakarya.djennati@mail.univ-tlemcen.dz

---

## 1. INTRODUCTION

The InAlAs/InGaAs/InP pseudomorphic high electron mobility transistors (pHEMT) have exhibited excellent performances in terms of noise figure compared to MOSFET devices at RF and microwave fields [1]. In addition, they are mostly used in the design of low noise amplifiers [2-4] and proven to be more advantageous than the AlGaAs/InGaAs pHEMTs [5].

Advanced circuit design that uses pHEMT, needs precise and accurate noise models, especially for their application in low noise MMIC. Many noise models have been reported in the literature: the well-known Fukui's model [6], the equivalent noise temperature model by Pospieszalski [7] and the flicker noise model for HEMTs [8]. Many approaches on HEMT's noise parameters characterization were investigated [9-11].

In 1974, R.A. Pucel proposed a charge control based approach for a noise model in FET devices, the model is known as the PRC noise model [12]. Later in 1988, the model was used for HEMT devices in [13] and later improved by Zhi [14] where they included, in the PRC model, the temperature coefficients in order to calculate precise noise parameters for HEMTs.

In this paper, we try to predict the noise performances at high frequency of an InAlAs/InGaAs/InP pHEMT by extracting the basic noise parameters using two approaches: a physical modelling and a mathematical modelling. This work is organized as follows: first, we discuss the different sources of noise in the pHEMT devices. Then, we make use of ATLAS from SILVACO TCAD suite, to simulate the noise behavior of a fabricated InAlAs/InGaAs/InP 250 nm gate length pHEMT. Next, we describe the analytical model based on the 2-port small-signal equivalent circuit of the device mentioned before and we calculate the

P,R,C noise coefficients in order to extract the noise parameters. Finally, the modeled InAlAs/InGaAs/InP pHEMT is used to design a single stage low noise amplifier (LNA) for S-band frequencies.

## 2. pHEMTs

### 2.1. Noise Sources in pHEMTs

Every semiconductor device exhibits the basic noise mechanisms in a way that depends on its features and physical properties. There are five dominant noise mechanism in pHEMTs: (1) Thermal noise, generated by the parasitic resistances of gate, drain and source; (2) Diffusion noise, located in the channel when the pHEMT is operating in saturation mode; (3) G-R noise, due to electron-hole pair generated in the space-charge or by impact ionization; (4) Shot noise, due to the reverse biased gate current; (5) The flicker noise, neglected in this work since the studied pHEMT is dedicated to LNA applications. But still, there are at least two situations where the flicker noise affects microwave circuits: the up-conversion in mixers and the phase noise of HEMT oscillators [15].

### 2.2. Physical Modelling of Noise in pHEMT

The epitaxial structure of the studied InAlAs/ InGaAs/InP pHEMT in this paper is shown in Table 1; it is comparable to the fabricated pHEMT from [16], the gate length is 250 nm and a total gate width of 100  $\mu\text{m}$ , its layout consist of  $2 \times 50 \mu\text{m}$  fingers. The efficacy of the physical model of the structure in Table1 has been tested in a previous work [17] through a DC characterization where we obtained, by inverse modelling, DC performances matched to data measurements ( $I_{\text{DSS}}=56\text{mA}$  at  $V_{\text{DS}}=1.5\text{v}$  and  $V_{\text{GS}}=0\text{v}$ ;  $g_{\text{m,max}}=125 \text{ mS/mm}$ ).

Table 1. The Epitaxial Structure of the a 250 nm InGaAs/InAlAs/InP pHEMT

Material	Layer	Thickness
$\text{In}_{0.53}\text{Ga}_{0.47}\text{As}$	Cap	5 nm
$\text{In}_{0.52}\text{Al}_{0.48}\text{As}$	Barrier	15 nm
$\text{In}_{0.52}\text{Al}_{0.48}\text{As}$	Delta doping	1.2 nm
$\text{In}_{0.52}\text{Al}_{0.48}\text{As}$	Spacer 1	10 nm
$\text{In}_{0.7}\text{Ga}_{0.3}\text{As}$	Channel	14 nm
$\text{In}_{0.52}\text{Al}_{0.48}\text{As}$	Spacer 2	10 nm
$\text{In}_{0.52}\text{Al}_{0.48}\text{As}$	Delta doping	1.2 nm
$\text{In}_{0.52}\text{Al}_{0.48}\text{As}$	Buffer	450 nm
InP (S.I.) Substrate		

The physical model in ATLAS-Silvaco is represented as a two-port noiseless device with random voltage sources attached to its ports. These external voltage source are small and random, they produce the same voltage at the device's terminals as the intrinsic noise sources ( $V_1$  at the input and  $V_2$  for the output, (see Figure 1).

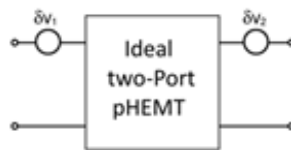


Figure 1. Block Diagram of the Modeled Noise Sources in pHEMT

ATLAS models the noise in the pHEMT, by calculating the statistical behavior of  $V_1$  and  $V_2$ . Two types of intrinsic noise were considered and defined with their parameters in the simulation: Diffusion noise and G-R noise couple with impact ionization noise.

A direct AC analysis was performed before the noise simulation; the current gain obtained is presented in Figure 2 where a good matching with data measurements is achieved. We believe that the physical model of the pHEMT is reliable and could be used in order to get an insight and estimation on the noise performances.

The noise simulation was performed on the pHEMT physical model under a bias point of  $15\%I_{\text{DSS}}$  to obtain the best noise performances. The spectral densities of the noise calculated at the input ( $V_1$ ) and the output ( $V_2$ ) of the device are presented in Figure 3.

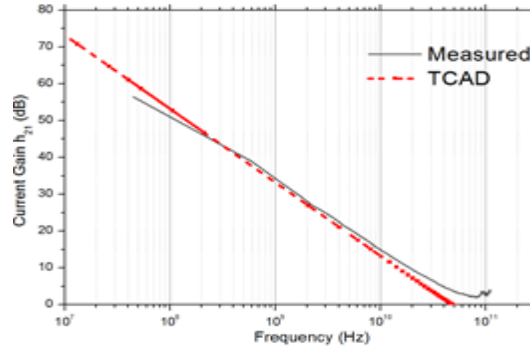


Figure 2. Current Gain (h21) vs Frequency, Simulated Against Measured at  $V_{GS}=0v$  and  $V_{DS}=1.5v$

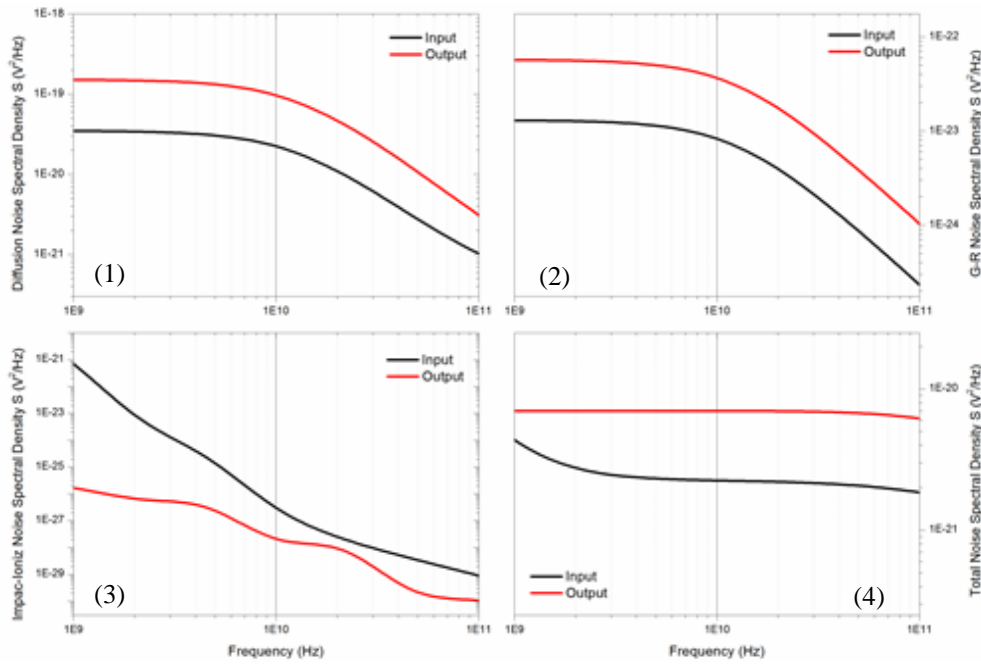


Figure 3. Voltage Spectral Density of: (1) Diffusion noise; (2) G-R noise; (3) Impact Ionization noise; (4) Total noise

### 2.3. Analytical Modeling

In The PRC analytical noise model in this work is based on the 2-port linear equivalent circuit shown in Figure 4. At the input, a gate current noise source  $i_g^2$  is in parallel with the output impedance composed of the channel charge resistance  $R_i$  in series with the gate-source capacitance  $C_{gs}$ , while in the output, a channel noise current source  $i_d^2$  is in parallel with the output resistance  $R_{ds}$ .

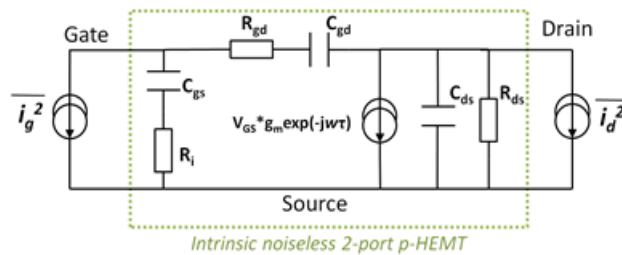


Figure 4. Intrinsic noiseless pHEMT equivalent circuit coupled with its noise sources

The elements of the small-signal equivalent circuit were calculated analytically from measured S-parameters charts, their values are presented in Table 2.

Table 2. Small-Signal Equivalent Circuit Parameters at T=300k with 15%I<sub>DSS</sub> and V<sub>DS</sub>=1v

R <sub>gd</sub> (Ω)	R <sub>i</sub> (Ω)	R <sub>ds</sub> (Ω)	C <sub>gd</sub> (fF)	C <sub>ds</sub> (fF)	C <sub>gs</sub> (fF)	g <sub>m</sub> (mS)	τ(pSec)
11	0.4	414.76	32	19.4	164	65	0.35
R <sub>g</sub> (Ω)	R <sub>s</sub> (Ω)	R <sub>d</sub> (Ω)	L <sub>g</sub> (pH)	L <sub>s</sub> (pH)	L <sub>d</sub> (pH)	C <sub>pg</sub> (fF)	C <sub>pd</sub> (fF)
1.49	0.60	0.67	35.7	3.0	92.4	11.2	36.7

The PRC terms in this model are dimensionless noise coefficients related to the magnitude of the current noise sources ( $i_g^2$  and  $i_d^2$ ), and to the correlation between them.  $P$  is referred to as the channel noise coefficient;  $R$  is the gate noise coefficient and last;  $C$  is the correlation coefficient between the gate noise current and the drain noise current. It should be noted that the correlation coefficient  $C$  is a pure complex parameter due to the existence of the coupling capacitance between the gate and the drain  $C_{gd}$ . The PRC coefficients are obtained by [12]:

$$P = \frac{\overline{i_d^2}}{4kT\Delta f g_m}, R = \frac{g_m \overline{i_g^2}}{4kT\Delta f \omega^2 C_{gs}^2}, C = \frac{Im(i_g i_d^*)}{\sqrt{(\overline{i_d^2} \overline{i_g^2})}} \quad (1)$$

The PRC coefficients were calculated using equations in (1) by considering the values of the small-signal equivalent circuit parameters in Table.1 with the values of  $i_g^2$  and  $i_d^2$  that were extracted from the simulation curves in Figure 3 ( $i_g^2$  is related to V1 and  $i_d^2$  related to V2). The results are shown in Figure 5.

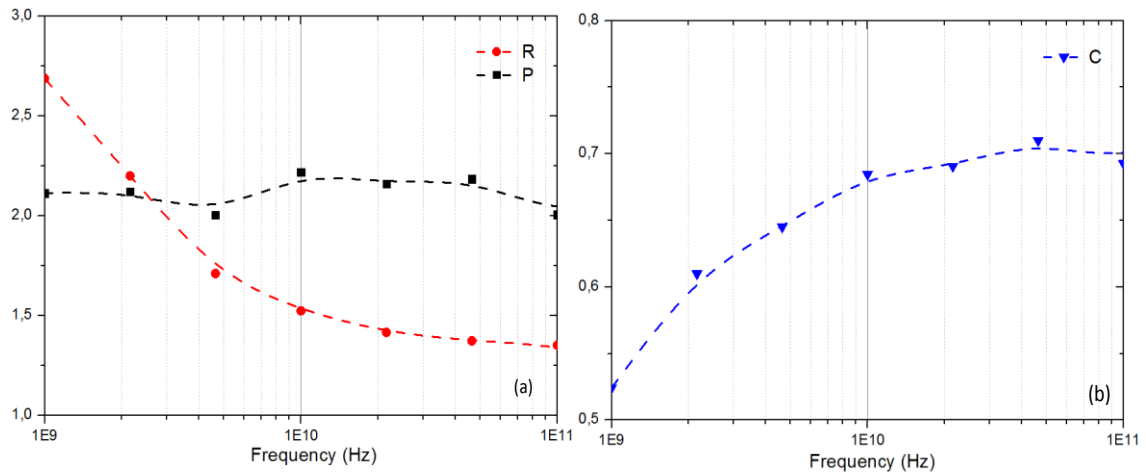


Figure 5. Values of P ,R and C Coefficients Versus Frequency of the 250nm InGaAs/InAlAs/InP pHEMT

The curves in Figure 5 are drawn in tendency lines due to the uncertainty in the calculation of the gate noise at a very low drain current value. Figure 5(a) shows a frequency independent drain noise coefficient  $P$  due to the hot electron effect in the channel. On the other hand, the gate noise coefficient  $R$  is frequency dependent for the relatively low frequencies region ( $<7\text{GHz}$ ): a result of an increasing in the gate leakage current. Concerning the correlation coefficient  $C$  shown in Figure 5(b), this parameter strongly depends on the gate's length  $L_g$ . We believe that the frequency dependence of the coefficients  $R$  and  $C$  is mainly linked to the shot noise caused by the reversed gate current. In addition to the PRC coefficients, three other parameters were described by Pucel:

$$K_g = P + R - 2C\sqrt{PR}, K_r = \frac{PR(1-C^2)}{P+R-2C\sqrt{PR}}, K_c = \frac{P-C\sqrt{PR}}{P+R-2C\sqrt{PR}} \quad (2)$$

The coefficients in (2) allow us to calculate the main noise parameters:

$$\left\{ \begin{array}{l} g_n = K_g \frac{\omega^2 C_{gs}^2}{g_m}, r_n = K_r \left( 1 + \frac{\omega^2 C_{gs}^2 R_i^2}{g_m} \right) \\ Z_c = R_c + jX_c = K_c \left( R_i - \frac{j}{\omega C_{gs}} \right) \\ R_n = r_n + g_n |Z_c|^2 \\ NF_{min} = 1 + 2g_n \left( R_c + \sqrt{R_c^2 + \frac{r_n}{g_n}} \right) \\ Re(Z_{opt}) = \sqrt{R_c^2 + \frac{r_n}{g_n}}, Im(Z_{opt}) = -X_c \end{array} \right. \quad (3)$$

The model above does not include the feedback capacitance  $C_{gd}$ , the charges held by this capacitance are responsible for the voltage drop in drain region. These charges also give a rise to gate leakage current component and therefore contribute to the noise behaviour of the device. When considering the effect of  $C_{gd}$ , the expressions of analytical model became as expressed in (4). The feedback capacitance  $C_{gd}$  added to the model in (4) constitutes a major influence in the noise figure: the coupling capacitance make the drain noise current frequency dependent resulting to a rise in noise figure for frequencies beyond  $f_t$  [18].

$$\left\{ \begin{array}{l} NF_{min} = 1 + 2 \frac{\omega(C_{gs}+C_{gd})}{g_m} \sqrt{K_r K_g} + 2 \frac{\omega^2(C_{gs}+C_{gd})^2}{g_m} K_r K_g R_i \\ R_n = \frac{P}{g_m} + \frac{\omega^2(C_{gs}+C_{gd})^2 (K_g K_c^2 + K_r^2) R_i^2}{g_m} \\ Re(Z_{opt}) = \sqrt{\frac{K_r}{K_g \omega^2 (C_{gs}+C_{gd})^2} + K_c^2 R_i^2}, Im(Z_{opt}) = \frac{K_c}{\omega C_{gs}} \end{array} \right. \quad (4)$$

### 3. RESULTS AND DISCUSSIONS

For a precise prediction of the device's noise performances, a precise noise model is needed. In this section, we extract and compare the main important noise parameters: the minimum noise figure  $NF_{min}$ , the equivalent noise resistance  $R_n$  and the optimum source impedance  $Z_{opt}$ . The curves of the mathematical model illustrate a good matching within the predicted range by TCAD simulation. While both model and TCAD curves are matched in  $NF_{min}$  and  $Z_{opt}$ , an average matching was achieved in  $R_n$ , nevertheless, the decreasing slop was correctly predicted. ATLAS-SILVACO uses the impedance field method, to determine the internal noise parameters in Figure 6, by characterizing the entire device's behaviour based on the fluctuation of the two correlated equivalent noise sources. Figure 6(a) shows a frequency dependence of  $NF_{min}$  at 15% IDSS. An increase from 0.7 dB to 1.2 dB is observed for frequencies less than 10 GHz, these values are well known for devices with a gate width of 100  $\mu m$ . In Figure 6(b), a considerable decrease of the noise resistance mainly due to the combined effect of a higher transconductance and a reduced gate noise coefficient.

However, the sheet carrier density values, the diffusion coefficients and the Generation-Recombination parameters needed to be adjusted in order to achieve a good matching of the pHEMT's noise parameters. The physical modelling offers a better insight on the physical mechanisms controlling the noise. Meanwhile, the mathematical model depends on the small-signal equivalent circuit elements, which is advantageous for pHEMT's optimization and improvements for its implementation in microwave circuits such as LNAs (low noise amplifiers). In addition, in the low-noise application, the pHEMT is generally embedded in the circuit and the values of the parasitic capacitances in the equivalent circuit will differ from the discrete elements used in this characterization, but the intrinsic elements still remain the same. Also, the access resistances especially the input access resistance  $R_g$ , will obviously generate thermal noise contributing to the overall noise figure. So from the low noise circuit designing perspective, it will be more useful to provide the whole model including the effect of access resistances. However we believe that the presented analytical model is straightforward solution to predict the noise behavior of pHEMTs during its design process.

Following the noise modeling, the parameters of the small-signal equivalent circuits of the 250nm 2x50 $\mu m$  pHEMT were to design a single stage LNA for S-band applications. The purpose was to demonstrate the potential of InAlAs/InGaAs/InP pHEMT in low noise applications.

The corresponding single stage LNA schematic along with the values of the passive components and the biasing conditions are illustrated in Figure 7. It is designed to operate in a frequency range of 2.4 GHz to

4.2 GHz in 50Ω system. The common source configuration of the LNA is has a noise figure close to the transistor’s minimum noise figure [19],[20] and it is less prone to oscillations than other topologies.

A high gate resistance was used to at the input terminal of the transistor to prevent large current flowing to the input and hence an optimum gate voltage injection is achieved. The series capacitors  $C_{in}$  and  $C_{out}$  isolate the DC bias sources for the RF input and RF output respectively. The drain capacitor  $C_D$  improves the input return loss and provides an output matching for the LNA. The resistor  $R_{D1}$  is used to prevent oscillations; however, it can reduce the overall gain to the amplifier and needs to be minimized.  $L_D$  and  $R_{D2}$  provide an adequate output match network and ensure the stability of the amplifier. The LNA has been implemented in the FET lineal model from ADS Agilent. The performances obtained are shown in Figure 8.

The amplifier shown in Figure 8(a), exhibited a gain around 12.6dB at the frequency of 3GHz, with a return loss coefficient at the input -2.4dB and grater that -7dB at the output as illustrated in Figure 8(c). The minimum noise figure and the noise factor in Figure 8(b), are less than 1dB for all the operating frequencies as predicted by the noise characterization in Figure 6(a). In must be noted that the passive components of the LNA are considered ideal. The results obtained can be used for accurate design with real process design kit.

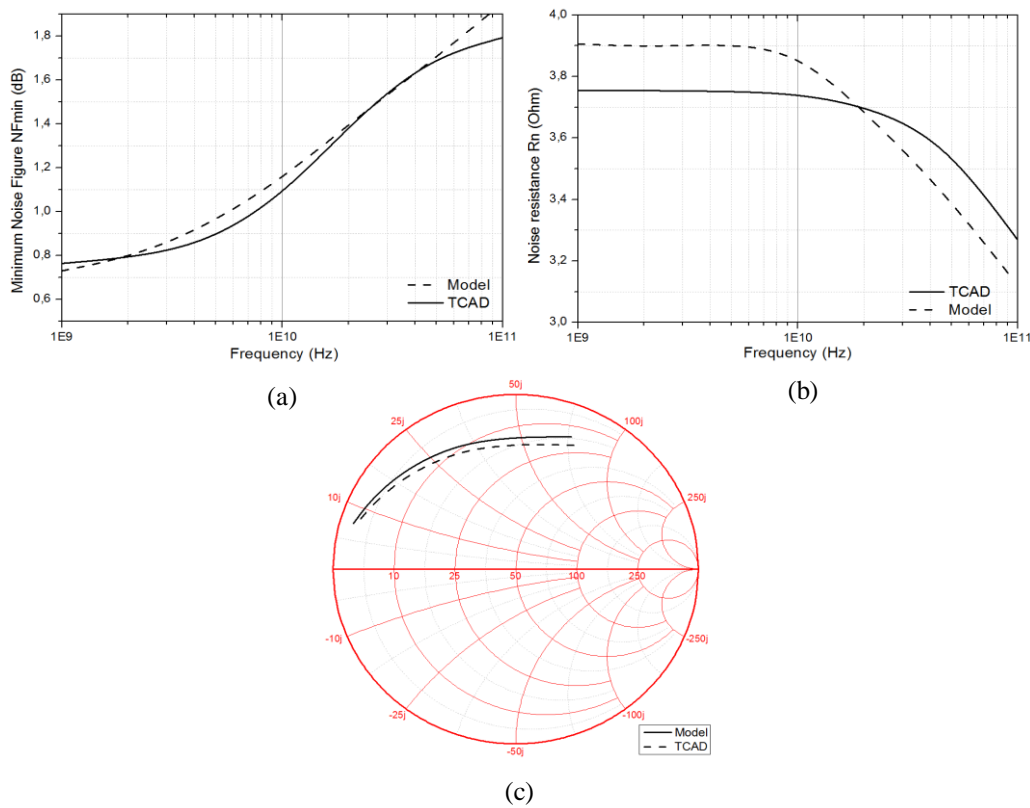


Figure 6. Plots of  $NF_{min}$  vs. frequency (a);  $R_n$  vs. frequency (b) and  $Z_{opt}$  chart (c) of the 250nm InAlAs/InGaAs/InP pHEMT

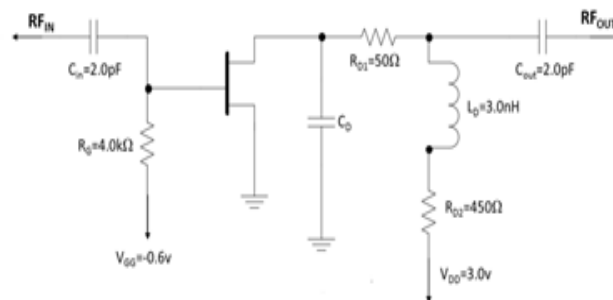


Figure 7. Schematic Circuit of Single Stage S-band Low Noise Amplifier

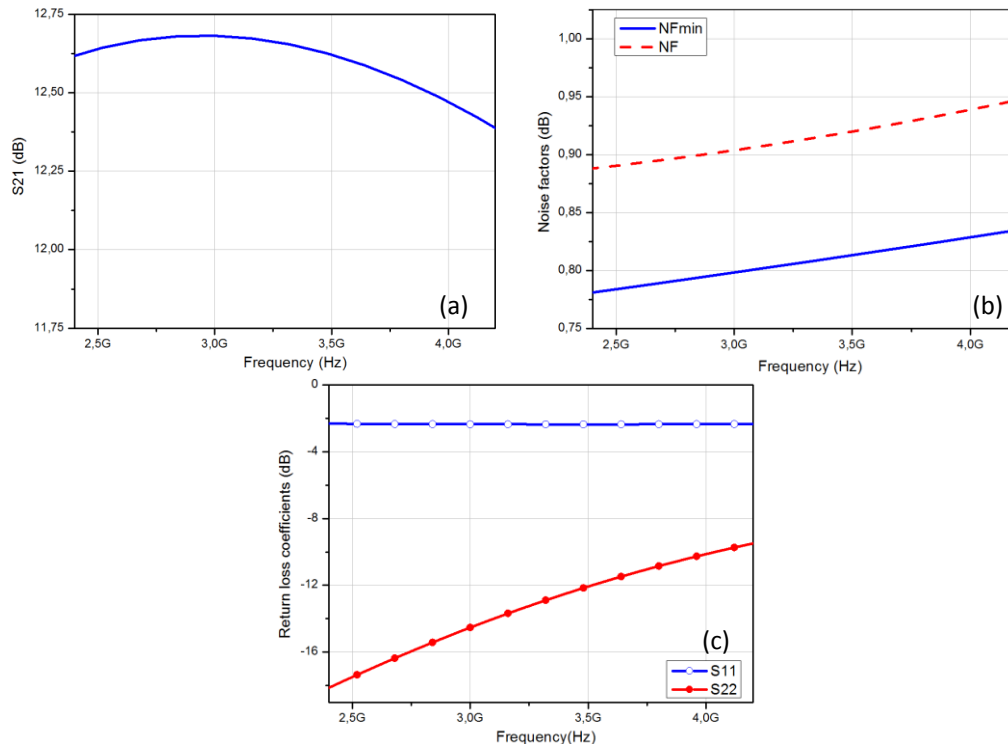


Figure 8. Performances of Single Stage LNA: (a) gain; (b) Noise figure; (c) Return Loss Coefficients

#### 4. CONCLUSION

In this work, a noise characterization was performed on InAlAs/InGaAs/InP pHEMT using two approaches: Pucel's PRC model based on analytical equations and a physical modelling by simulation on Atlas-Silvaco. We observed that both mathematical and physical model can predict the noise performances of InAlAs/InGaAs/InP pHEMTs. The improved analytical model and the physical model were adjusted to obtain matching results between the main noise's parameters ( $NF_{min}$ ,  $R_n$  and  $Z_{opt}$ ) in a wide frequency range (1-100GHz). A single stage S-band LNA was simulated from the small signal equivalent circuit. The LNA demonstrated a gain of 12.6dB and a noise figure less than 1dB as predicted. Future work will be devoted to model the thermal noise by including temperature variation in order to have a full insight on the noise performances of InAlAs/InGaAs/InP pHEMT.

#### ACKNOWLEDGEMENTS

The authors wish to thank Professor M. Missous from the school of Electrical and Electronic Engineering at Manchester's University, for providing the pHEMT structure and data measurements used for this work.

#### REFERENCES

- [1] F. Danneville, "Microwave noise and FET devices," *IEEE Microw. Mag.*, vol/issue: 11(6), pp. 53–60, 2010.
- [2] D. H. Kim and J. A. D. Alamo, "30-nm InAs pseudomorphic HEMTs on an InP substrate with a current gain cutoff frequency of 628 GHz," *Electron Device Letters, IEEE*, vol. 29, pp. 830-833, 2008.
- [3] F. Packeer, *et al.*, "Fabrication and characterization of tensile InAlAs barrier and compressive InGaAs channel pHEMTs having extremely low gate leakage for low-noise applications," *J. Phys. D: Appl. Phys.*, vol. 49, pp. 1-3, 2013.
- [4] H. Wang, *et al.*, "Fully passivated W-band InAlAs/InGaAs/InP monolithic low noise amplifiers," *IEE Proceedings - Microwaves, Antennas and Propagation*, 1996.
- [5] S. Arshad, *et al.*, "Modelling of the Kink Effect in Strained InGaAs/InAlAs pHEMTs," pp. 55-58, 2008.
- [6] H. Fukui, "Optimal noise figure of microwave GaAs MESFETs," *IEEE Transactions on Electron Devices*, vol. 26, pp. 1032-1037, 1979.
- [7] M. W. Pospieszalski, *et al.*, "Interpreting Transistor Noise," *Microw. Mag.*, 2010.

- [8] A. van der Ziel, "1/f Noise in HEMT type GaAs FETs at low drain bias," *Solid State Electron*, vol/issue: 26(5), pp. 385–386, 1983.
- [9] A. Nalli, *et al.*, "GaN HEMT noise model based on electromagnetic simulations," *IEEE Trans on Microwave Theory and Technique*, vol. 4, pp. 2498–2508, 2015.
- [10] Z. Kourdi, *et al.*, "Side Effects in a HEMT Performance with InAlN/GaN," *TELKOMNIKA Indonesian Journal of Electrical Engineering*, vol/issue: 15(2), pp. 249–258, 2015.
- [11] S. Colangeli, *et al.*, "Polynomial noise modelling of silicon based GaN HEMTs," *Int. J. Numer. Model. Electron. Netw. Devices Fields*, vol/issue: 27(5–6), pp. 812–821, 2013.
- [12] R. A. Pucel, *et al.*, "Signal and noise properties of gallium arsenide microwave field effect transistors," *Adv. Electron. Electron Phys.*, vol. 38, pp. 195–265, 1975.
- [13] A. Cappy, "Noise modelling and measurement techniques," *IEEE Trans. Microwave Theory Tech.*, vol/issue: 36(1), pp. 1–10, 1988.
- [14] Z. H. Liu, *et al.*, "Analytical Modeling of High-Frequency Noise Including Temperature Effects in GaN HEMTs on High-Resistivity Si Substrates," *IEEE Trans. Electron Devices*, vol/issue: 57(7), pp. 1486–1491, 2010.
- [15] T. Felgentreff and G. R. Olbrich, "Modelling of low frequency noise sources in HEMTs," in *proceeding of IEEE MTT-S International Microwave Symposium Digest*, 1996.
- [16] K. Ian, *et al.*, "Thermally stable InGaAs/InAlAs pHEMTs using thermally evaporated palladium gate metallization," *Semicond. Sci. Technol.*, vol. 29, pp. 1–5, 2014.
- [17] Z. A. Djennati, *et al.*, "2-D Physical Modeling and DC Optimization of a double delta doped In<sub>0.7</sub>Ga<sub>0.3</sub>As/In<sub>0.52</sub>Al<sub>0.48</sub>As/InP pHEMT," in *Proc. Advanced topics in electrical engineering. Symp., Bucharest, Romania*, pp. 889–901, 2015.
- [18] V. Guru, *et al.*, "Analytical noise model of a high-electron-mobility transistor for microwave-frequency application," *Microw. Optoelectr. Technol. Lett.*, vol/issue: 40(5), pp. 410–417, 2004.
- [19] A. B. Ibrahim, *et al.*, "Low Noise Amplifier at 5.8GHz with Cascode and Cascaded Techniques Using T-Matching Network for Wireless Applications," *International Journal of Electrical and Computer Engineering*, vol/issue: 1(1), pp. 1–8, 2011.
- [20] K. Pongot, *et al.*, "Design and Analysis High Gain PHEMT LNA for Wireless Application at 5.8 GHz," *International Journal of Electrical and Computer Engineering*, vol/issue: 5(3), pp. 611–620, 2015.